Optics Letters

System design of a single-shot reconfigurable null test using a spatial light modulator for freeform metrology

Romita Chaudhuri, Jonathan Papa, and Jannick P. Rolland*

The Institute of Optics, University of Rochester, 275 Hutchison Road, Rochester, New York 14620, USA
**Corresponding author: rolland@optics.rochester.edu*

Received 4 February 2019; revised 13 March 2019; accepted 14 March 2019; posted 14 March 2019 (Doc. ID 359498); published 9 April 2019

We report the simulation of an adaptive interferometric null test using a high-definition phase-only spatial light modulator (SLM) to measure form and mid spatial frequencies of a freeform mirror with a sag departure of 150 μm from its base sphere. A state-of-the-art commercial SLM is modeled as a reconfigurable phase computer generated hologram (CGH) that generates a nulling phase function with close to an order of magnitude higher amplitude than deformable mirrors. The theoretical uncertainty in form measurement arising from pixelation and phase quantization of the SLM is 50.62 nm RMS. The calibration requirements for hardware implementation are detailed.

https://doi.org/10.1364/OL.44.002000

Freeform optics refer to surfaces without rotational or translational symmetry, with arbitrary sag departure from a base plane, sphere, toroid, or conic. Unlike off-axis conics, freeform surfaces allow higher degrees of freedom in optical design independent of surface geometry, which enables improved performance along with miniaturization of optical systems (e.g., wide field-of-view telescopes [1], spectrometers [2], head-worn displays [3], and illumination applications [4]). The widespread utilization of freeform surfaces in optical systems is critically dependent on the availability of non-contact, flexible, and preferably economic metrology tools with low ($\leq$ 1 μm and ideally approaching tens of nm) uncertainty in form measurements. Non-contact metrology techniques are classified into point-cloud and full-field methods based on the modality of acquisition of measurement data. Swept-source optical coherence tomography (SS-OCT) is an example of a point-cloud metrology technique with measurement uncertainty on the order of 100 nm for 1-in. diameter optics [5]. However, SS-OCT may suffer from excessive noise caused by mechanical scanning of the sample. Commercial point-cloud optical profilometers can measure larger optics with extreme slopes enabled by a large range of mechanical scanning [6]. In all these point-cloud techniques, the time for data acquisition scales with the size of the part and the density of sampling. Development of part-independent full-field metrology techniques is an area of active research using single-shot data acquisition and elimination of mechanical scanning. Structured light illumination [7] and phase measuring deflectometry (PMD) [8] are examples of full-field metrology techniques involving slope integration to reconstruct the shape of freeform surfaces with high asphericities with micrometer-level uncertainty [9]. Tilted wave interferometry [10] and transverse translation diverse phase retrieval are other emerging freeform metrology techniques [11].

The current industry standard to measure rotationally variant optics is an interferometric null test, being a non-contact, full-field technique that achieves nanometer-level uncertainty in form measurements. Direct, on-axis interferometry is not suitable to measure anything other than a spherical surface due to the high density of fringes that cannot be resolved [12]. Thus, interferometric null tests for measuring freeform optical mirrors typically involve a custom null element such as a computer generated hologram (CGH) [13] or an adaptive null using a deformable mirror (DM) [14,15], sometimes in combination with additional custom null elements. While the CGH-based null test can test a few hundreds of microns of freeform sag departure of the test optic, it is part-specific and involves significant expense and lead time for fabrication. In contrast, the DM-based null test is adaptive and economical compared to CGHs; however, DMs are limited by the stroke of the actuators [16] and consequently compensate only mild freeform departures.

A high-definition (i.e., >1080 pixels, <5 μm pitch) spatial light modulator (SLM) circumvents the limitation of the DM by phase wrapping to generate larger than 2π radian phase, as demonstrated in the correction of aberrations in human eyes [17] or compensating atmospheric turbulence [18]. In optical testing, SLMs have been used to correct (1) power in progressive addition lens [19], and (2) <1 wave of aberrations on a thin flat membrane mirror [20], both in Shack–Hartmann test configurations. Recently, an SLM was used to null unknown localized deformations over a sub-aperture of an optic in combination with a part-specific null such as a CGH or an Offner null to compensate the nominal freeform departure from a flat [21].

In this Letter, we report an interferometric null test architecture with a high-definition SLM used as a standalone nulling

element for full-field and single-shot form measurement of free-form optics. Single-shot measurement implies that the SLM is not translated to generate the full-aperture surface measurement. The state-of-the art in SLMs (e.g., Holoeye GAEA2 with 4160 × 2464 pixels [22]) enables the generation of wavefronts with peak-valley (PV) of a few hundreds of microns [23], which is modeled in the simulation of the proposed null test architecture.

The Nyquist sampling criterion requires at least 2 pixels per period of the wrapped phase displayed on the SLM, which determines the maximum slope $\theta_{\max}$ and peak-valley (PV) of the wavefront $W_{\max}$ that the SLM can generate. Using the pixel pitch p and the space-bandwidth (SW) product (i.e., number of pixels N) of the SLM, $\theta_{\max}$ is calculated as $\tan^{-1}(\lambda/(2*p))$, and $W_{\max}$ is $N*\lambda/2$, where λ is the operating wavelength. For the Holoeye GAEA2, N is 2464 along the short axis of the SLM and p is 3.74 μm. At λ of 632.8 nm, the calculated $W_{\max}$ equals 779.6 μm, and the $\theta_{\max}$ equals 4.84°. Here, the calculated $W_{\max}$ is much higher than that generated by a typical DM that reaches a maximum of ∼50 μm PV (tilt wavefront).

The general schematic for the SLM-based null test configuration is shown in Fig. 1(a). A commercial Fizeau interferometer emits a collimated test beam at 632.8 nm, which is de-magnified to a beam diameter of 9.22 mm equal to the length of the short axis of the SLM through a 4:1 beam expander, and a quarter-wave plate converts the circular polarization to linear polarization parallel to the SLM long axis. The SLM is slightly tilted to clear the reflected beam from the interferometer. A singlet lens is placed after the SLM to image the SLM on the optic under test (OUT). Let us denote the radius of curvature (r.o.c) of a "best-fit sphere" of the freeform as R_s. The best-fit sphere is defined as the sphere that fits the surface resulting in minimum peak-valley sag departure. Placing the optic concentric to the best-fit sphere removes the power, and the residual sag departure is nulled by the conjugate nulling wavefront applied to the SLM. The phase kinoform formed by wrapping the nulling phase between 0 and 2π radian is designed for maximum efficiency in the +1 order at the test wavelength. A tilt carrier is added to the phase kinoform to separate the diffraction orders. Irises are employed at the focal plane of the lenses to block the unmodulated zero order and the diffraction orders other than the +1 order. A null interferogram is generated when the departure of the optic from the best fit sphere is compensated by the phase function on the SLM.

The principle of operation of the SLM-based null test is similar to the CGH-based null test since both methods employ a diffractive null to compensate the departure of the optic from a sphere/plane. However, the key advantage of the SLM-based method is that it is reconfigurable unlike the CGH which is custom-made for each OUT. The reconfigurability of the SLM makes it much more economical compared to the CGH and eliminates the lead time for fabrication of the CGH. CGH-based technology is discussed in [12]. Another key advantage of the SLM-based null test is that the SLM is imaged to the OUT unlike typical CGH-based null test configurations where the non-linear mapping of the optic to the CGH due to improper imaging result in measurement errors [24].

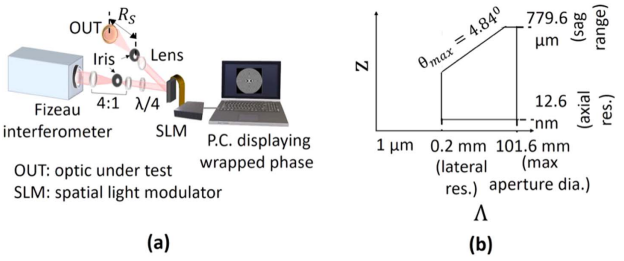

Fig. 1. Illustration of the SLM-based null test showing (a) system layout (not drawn to scale), and (b) Stedman diagram (sag range "z" versus spatial wavelength "Λ"), representing the metrology capability.

Prior work using a deformable mirror in a null test paved the way for adaptive techniques in freeform optical metrology [14]. Here, we investigate in simulation an SLM-based null test, leveraging unique features of the rapidly emerging SLM technology: (1) The high wavefront range of the SLM eliminates the refractive Offner-null to correct spherical aberration; (2) nulling the power enables the SLM to completely compensate the residual departure of the optic, without tilting it to null astigmatism. This is a key advantage, given that a custom-made Kelvin clamp was used to precisely maintain the tilt of the optic at the angle calculated from the Coddington equation in the DM-based test [14]. The on-axis testing of the optic significantly eases the alignment and distinguishes between wavefront errors induced by form errors as opposed to those induced by misalignment; (3) alignment fiducials can be displayed over the full aperture of the SLM, which will ease aligning the SLM to the optic before testing with the nulling wavefront; (4) the test beam is incident twice on the SLM but only once on the OUT, reducing the amplitude of the nulling wavefront to half of that required in the DM-based null test. This feature efficiently utilizes the wavefront range of the SLM for nulling severe departures.

The metrology capability of the method is represented on a log-log plot of sag amplitude (z) versus spatial wavelength (Λ), known as Stedman diagram [25], shown in Fig. 1(b) for our system. The maximum sag departure of the OUT that can be nulled by the SLM (including the added tilt carrier) is the $W_{\max}$ of 779.6 μm calculated earlier. The minimum measurable sag departure (i.e., noise floor of the system, $z_{\min}$) is dominated by the phase flicker, which is a characteristic of digitally addressed SLMs. For the Holoeye GAEA2, the flicker is PV 2% of 2π phase, i.e., 12.6 nm.

The mid-spatial frequency (MSF) spatial periods are typically considered to span from >5 cycles/aperture to the period corresponding to a Fresnel number of <0.1 (far field regime). For optics with diameter in the order of 5 in., the MSF spatial wavelengths are in the range of 2–0.2 mm from a fabrication perspective. To resolve the smallest MSF period, at least 2 pixels of the SLM should be imaged over a spatial period of 0.2 mm on the part, scaled by the magnification of the lens ($D_{\text{optic}}/D_{\text{SLM}}$), such that

$$2*p*\frac{D_{\text{optic}}}{D_{\text{SLM}}} \le 0.2 \text{ mm}, \quad \textbf{(1)}$$

where p equals 3.74 μm is the pixel pitch, D_{optic} is the part diameter, and D_{SLM} equals 9.22 mm is the length of the short axis of the SLM. For D_{optic} equal to 127 mm (i.e., 5 in.), the left-hand side of Eq. (1) equals 0.1 mm, satisfying the condition to resolve the MSF periods. Thus, the lateral resolution of the null test system (i.e., 2*pixel size on the part) is limited by the camera of the interferometer which has lesser number of pixels than the SLM.

A typical commercial Fizeau interferometer has 1200 × 1200 pixels over 6× zoom. For a 4-in. test beam diameter, the pixel size on the part ranges from 14 μm for 6× zoom and up to 84.7 μm for 1× zoom. Thus, the lateral resolution of the system is 0.17 mm (i.e., 2*84.7 μm) for 4-in. optics and even better for smaller optics. The iris is set to fully pass the +1 diffraction order while blocking the other orders and, as such, does not affect the measurement bandwidth.

While the reconfigurability of the SLM enables the measurement of a wide range of surface types (including toroids, off-axis conics, and aspheres), we report here the simulation of the null test of a freeform mirror as the generalized case. The freeform mirror has a clear aperture of 101.6 mm (4 in.), surface sag of 3.2 mm, and maximum slope of 7.4°. This OUT has a base sphere r.o.c. of −400 mm, and the freeform sag component is composed of astigmatism and coma, which are described by Fringe Zernike polynomial coefficients.

In the optical design software, the OUT was placed concentric to a point source at a distance equal to the r.o.c of the base sphere (i.e., $R_s = -400$ mm) as a starting point and was optimized for minimum RMS wavefront error. The value of R_s remained equal to −400 mm after optimization, indicating that for this freeform mirror the base sphere is the best-fit for minimum sag departure, which may not be the case for freeforms with a base conic. Figure 2(a) shows the residual sag departure of the OUT from the best-fit sphere, with a PV sag of 150 μm and a maximum slope of 0.23°.

The focal length f of the imaging singlet was calculated according to $R_S * D_{\mathrm{SLM}}/D_{\mathrm{optic}}$, which equals 36.3 mm for D_{SLM} of 9.22 mm and D_{optic} of 101.6 mm. A singlet with a high refractive index material (Schott NSF6), f of 36.3 mm, and entrance pupil diameter of 9.22 mm was optimized for minimum RMS wavefront error, resulting in 0.72λ PV wavefront aberrations at 632.8 nm. The null test layout in the software is shown in Fig. 2(b), with the OUT at a distance R_s from the focal plane of the lens and the SLM at the conjugate distance of 33 mm. The SLM was modeled as a reflective phase kinoform tilted at 12° with respect to the incident beam. The small tilt of the SLM minimizes phase errors that would be caused by a large angle of incidence on the SLM [26]. The nulling wavefront on the SLM was described by X-Y polynomial coefficients corresponding to a phase kinoform designed for 100% diffraction efficiency in the +1 order at 632.8 nm. The interferogram with a PV of 479.14λ before correction by the SLM (scaled 40× for visibility) is shown in Fig. 2(b).

The X-Y polynomial coefficients on the SLM were optimized to solve for the wavefront that nulls the departure of the OUT and the aberrations of the lens. Figure 3(a) shows the schematic

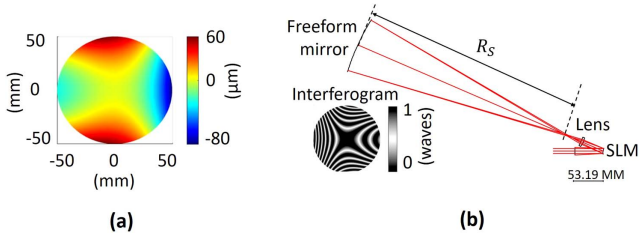

Fig. 2. Illustrations before optimization of the SLM showing (a) the freeform sag departure of the optic from the base sphere, (b) the null test layout in optical design software with the SLM switched off, and (inset) the corresponding interferogram (scaled 40×).

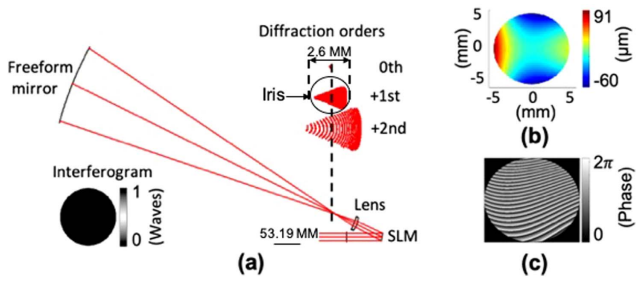

Fig. 3. Illustrations after optimization of the SLM: (a) null test showing the separation of diffraction orders and the generated null interferogram, (b) the optimized nulling wavefront, and (c) the wrapped nulling phase function on the SLM with the tilt carrier superposed (scaled 50× for visibility).

with the SLM displaying the optimized wavefront and the null interferogram obtained with a PV of 0.008λ. The optimized nulling wavefront with 151.59 μm PV is shown in Fig. 3(b). The phase applied to the SLM is generated by applying a tilt carrier to the nulling wavefront and phase wrapping between 0 and 2π as shown in Fig. 3(c) (scaled 50×). The tilt carrier separates the diffraction orders and a 2.6 mm diameter iris at the focal plane of the lens fully passes the +1 order while blocking all other orders, as shown in Fig. 3(a). The nulling wavefront including the tilt carrier has a PV of 570.12 μm and a maximum slope of 4.84°, which are compliant with the values of $W_{\max}$ and $\theta_{\max}$ at the Nyquist limit.

The diffraction efficiency (η) of the displayed phase is a function of the number of pixels within the period of the wrapped phase. The number of pixels per period varies over the displayed phase function non-linearly, with the minimum diffraction efficiency of 40.53% ($\eta = 0.4$) at the Nyquist limit of two pixels per period. In practice, the high (90%) fill-factor of the GAEA2 SLM will slightly reduce η by a few percent [27], which will still round up to $\eta = 0.4$. The value of η influences the intensity of the test beam (I_{test}) that interferes with the reference beam after propagation through the test beam path. For high-contrast fringes, I_{test} needs to be close to 4% of the source intensity (I), or $0.04 * I$, which is the intensity of the reference beam, i.e., the 4% Fresnel reflection from the transmission sphere. The value of I_{test}:

$$I_{\mathrm{test}} = 0.96I * (T_{\mathrm{BE}}^2 * T_{\mathrm{WP}} * R_{\mathrm{SLM}} * \eta * T_{\mathrm{lens}}^2)^2 * R_o, \quad \textbf{(2)}$$

where $0.96 * I$ is the intensity of the test beam from the interferometer after Fresnel reflection, T_{WP} is the transmittance of the quarter-wave plate, R_{SLM} is the reflectance of the SLM, and R_o is the reflectance of the optic. T_{lens} is the transmittance of each surface of the lens, and T_{BE} equals T_{lens}^2 is the transmittance of each lens in the beam expander, which is of the same material as the lens. At 632.8 nm, T_{wp} equals 0.98, R_{SLM} equals 0.62, T_{lens} for Schott NSF6 equals 0.998, and R_o equals 0.9, which yields I_{test} to be $0.05 * I$. Thus, the minimum test beam intensity is $0.045 * I$, which is compliant with the intensity requirement for high contrast fringes. Variation of η over the beam does not impact the wavefront measurement through quadrature phase-shifting, which involves the calculation of the pixel-wise phase change.

The simulations in optical design software generate the nominal nulling wavefront to be applied to the SLM to generate a

perfect null. In practice, the SLM will have inherent aberrations in the order of $<2\lambda$ PV, which will be nulled by applying a compensation map. Since these aberrations are specific to the SLM used and are very small, applying the wavefront compensation will not significantly alter the wavefront range $W_{\max}$ of the SLM. The SLM will also be calibrated for compensating the non-linearity of the gamma curve and the non-uniformity of the SLM backplane [28] to minimize the error in the generated wavefront by the SLM. Also, errors arise due to pixelation of the SLM that produces a stair-case approximation to the continuous wavefront designed in software. In addition, the wavefront is quantized to 256 levels (between 0 and 2π phase). Since the SLM is conjugated to the optic, the error introduced by the pixelation and quantization on the null test is analyzed at the SLM plane itself without propagating it to the plane of the optic. First, the 2D nulling wavefront was generated over an array size of three times the number of pixels on the SLM to approximate the continuous wavefront with a very high density of sampling (7392×7392 points over the beam diameter on the SLM). Then, to emulate the pixelation of the SLM, six adjacent simulation points (three points along X and Y directions each) were assigned the average value of the corresponding six points in the highly sampled wavefront. Next, the phase (ϕ) corresponding to the pixelated wavefront is quantized into 256 levels representing 0 to 2π phase yielding the quantized phase (ϕ_q)

$$\phi_q = \text{Round}\left(\phi * \frac{255}{2\pi}\right) * \frac{2p}{255}. \tag{3}$$

The difference between the highly sampled wavefront and the pixelated, quantized wavefront yields an error of $\pm 0.14\lambda$ (RMS error of 0.04λ). Due to double incidence on the SLM, the estimated residual in the null test is two times the calculated error, i.e., $\pm 0.28\lambda$ and RMS of 0.08λ (50.62 nm).

In practice, the wavefront generated by the SLM will be measured using a wavefront sensor, and the difference between the wavefront generated by the SLM and the simulated nulling wavefront will be subtracted from the measurment of the optic. This strategy minimizes the uncertainty in the null test measurements due to wavefront error from the SLM, similar to the closed-loop feedback employed in DM-based null tests [14,15] for calibrating out the error in the DM's shape from the null test measurement.

The beam expander and the imaging singlet will be custom-made to PV $\lambda/20$ surface quality and will be tested interferometrically. The simulated phase function already compensates the aberrations introduced by the designed lens, and any additional wavefront error from the lens characterization will be calibrated out of the null test results.

In summary, the system design of a reconfigurable, single-shot SLM-based full-field interferometric null-test for the measurement of freeform mirrors is reported. The maximum sag measurable is a function of the number of pixels on the SLMs and will be higher for future generations of SLMs. Freeforms of larger or smaller size can be tested using a lens with the suitable magnification, provided that the maximum slope of the nulling wavefront, including the tilt carrier, is within the Nyquist limit of the SLM. The unique features of SLM-based testing, such as the lack of custom null optics, on-axis testing, and the ability to display fiducials to facilitate alignment are promising as a completely reconfigurable metrology technique.

Funding. II-VI Foundation (Block Gift Program).

Acknowledgment. This research synergizes with the Center for Freeform Optics (CeFO) (IIP-1338877, IIP-1822049, IIP-1338898, IIP-1822026). We thank Synopsys, Inc. for the education license of CODE V, and Di Xu, Yves Surrel, Konstantinos Falaggis, and Rosario Porras-Aguilar for stimulating discussions.

REFERENCES

1. A. Bauer, E. M. Schiesser, and J. P. Rolland, Nat. Commun. **9**, 1756 (2018).
2. J. Reimers, A. Bauer, K. P. Thompson, and J. P. Rolland, Light Sci. Appl. **6**, e17026 (2017).
3. A. Bauer and J. P. Rolland, Opt. Express **22**, 13155 (2014).
4. X. Wu, G. Jin, and J. Zhu, Appl. Opt. **56**, 2405 (2017).
5. J. Yao, A. Anderson, and J. P. Rolland, Opt. Express **26**, 10242 (2018).
6. S. Defisher, in *Imaging and Applied Optics*, OSA Technical Digest (Optical Society of America, 2015), paper JT5A.6.
7. J. Geng, Adv. Opt. Photon. **3**, 128 (2011).
8. M. C. Knauer, J. Kaminski, and G. Hausler, Proc. SPIE **5457**, 366 (2004).
9. L. R. Graves, H. Choi, W. Zhao, C. J. Oh, P. Su, T. Su, and D. W. Kim, Opt. Lett. **43**, 2110 (2018).
10. G. Baer, J. Schindler, C. Pruss, J. Siepmann, and W. Osten, Opt. Express **22**, 31200 (2014).
11. A. M. Michalko and J. R. Fienup, Opt. Lett. **43**, 1331 (2018).
12. D. Malacara, *Optical Shop Testing*, 3rd ed. (Wiley, 2007).
13. J. C. Wyant and V. P. Bennett, Appl. Opt. **11**, 2833 (1972).
14. K. Fuerschbach, K. P. Thompson, and J. P. Rolland, Opt. Lett. **39**, 18 (2014).
15. L. Huang, H. Choi, W. Zhao, L. R. Graves, and D. W. Kim, Opt. Lett. **41**, 5539 (2016).
16. E. Dalimier and C. Dainty, Opt. Express **13**, 4275 (2005).
17. P. M. Prieto, E. J. Fernández, S. Manzanera, and P. Artal, Opt. Express **12**, 4059 (2004).
18. C. Rickenstorff, J. A. Rodrigo, and T. Alieva, Opt. Express **24**, 10000 (2016).
19. M. Ares, S. Royo, I. Sergievskaya, and J. Riu, Appl. Opt. **49**, 6201 (2010).
20. B. Yang, Y. Wei, X. Chen, and M. Tang, Proc. SPIE **9272**, 927218 (2014).
21. S. Xue, S. Chen, Z. Fan, and D. Zhai, Opt. Express **26**, 21910 (2018).
22. Holoeye Corporation, https://holoeye.com/gaea-4k-phase-only-spatial-light-modulator/.
23. R. Chaudhuri and J. P. Rolland, "Single-shot, adaptive metrology of rotationally variant optical surfaces using a spatial light modulator," PCT patent (October 2018).
24. P. Zhou, J. Burge, and C. Zhao, Proc. SPIE **7790**, 77900L (2010).
25. M. Stedman, Precis. Eng. **9**, 149 (1987).
26. A. Lizana, N. Martin, M. Estapé, E. Fernández, I. Moreno, A. Márquez, C. Lemmi, J. Campos, and M. J. Yzuel, Opt. Express **17**, 8491 (2009).
27. A. Jesacher, "Applications of spatial light modulators for optical trapping and image processing," Ph.D. dissertation (Leopold-Franzens University, 2007).
28. J. L. M. Fuentes, E. J. Fernández, P. M. Prieto, and P. Artal, Opt. Express **24**, 14159 (2016).